

**Electronic Supplementary Information for:
In vitro and *in vivo* biolasing of fluorescent proteins suspended in
liquid microdroplet cavities**

*Alexandr Jonáš^a, Mehdi Aas^b, Yasin Karadag^b, Selen Manioğlu^c, Suman Anand^d, David
McGloin^d, Halil Bayraktar^c, and Alper Kiraz^b*

^aDepartment of Physics, Istanbul Technical University, Maslak 34469, Istanbul, Turkey

^bDepartment of Physics, Koç University, Rumelifeneri Yolu, Sariyer 34450, Istanbul, Turkey

^cDepartment of Chemistry, Koç University, Rumelifeneri Yolu, Sariyer 34450, Istanbul,

Turkey

^dSchool of Engineering, Physics and Mathematics, University of Dundee, Nethergate,

Dundee DD1 4HN, UK

Experimental setups for fluorescence microspectroscopy and microscopy of surface-supported microdroplets

In the droplet lasing experiments reported in this article, individual surface-supported droplets were optically pumped with a pulsed 488 nm laser beam obtained by frequency-doubling the 976 nm output of an ultrafast Ti:Sa laser (pulse width 140 fs, repetition rate 80 MHz - Chameleon Ultra II; Coherent). Pump laser pulses were sent to the studied droplet in bunches of 5 μ s duration separated by 10 ms dark periods. To this end, output beam from the laser was focused through an aspheric lens L1 on a pinhole with \sim 155 μ m diameter located on a chopper wheel rotating with frequency of 100 Hz and then collimated again by a plano-convex lens L2 (see Fig. S1). After re-collimation, beam diameter was expanded four times with respect to its original size. The laser repetition rate of 80 MHz corresponds to the separation between the pulses of 12.5 ns and, thus, each 5 μ s excitation bunch contains on average 400 pulses (see Fig. S2). In order to minimize the distortion of the studied droplet shape by intense pump laser pulses, a single bunch of excitation pulses was typically used for recording an emission spectrum of the droplet. Single pulse bunches were selected by adding a mechanical shutter to the optical path of the pump beam and synchronizing it with the chopper wheel rotation using an auxiliary diode laser whose power was modulated by the chopper, detected by a photodiode, and fed to the computer controlling the experiment. The overall power of the pump beam could be adjusted by the combination of a half-wave plate and a polarizing beam splitter. After expansion, the excitation beam was reflected from a dichroic mirror and then focused at the rim of the studied droplet using a high NA water-immersion microscope objective lens (60x, NA = 1.2; Nikon) to a diffraction-limited spot with the radius of approximately 0.4 μ m. Fluorescence emission from the droplets was collected using the same microscope objective, transmitted through the dichroic mirror, and dispersed by a monochromator (focal length 500 mm; Acton Research) before detection by a

cooled spectroscopic CCD camera (Pixis 100; Princeton Instruments). For spectral acquisitions, spectroscopic CCD detector was synchronized with the mechanical shutter using electronic trigger line. Microdroplets deposited on the surface were imaged with an independent CCD camera placed at a different exit port of the microscope.

High-resolution images and videos of surface-supported microdroplets with suspended bacteria (see Fig. S6 for illustration) were recorded using an inverted optical microscope (IX83; Olympus) equipped with a high-NA oil-immersion objective lens (UPLSAPO 100x/1.4; Olympus) and an EMCCD camera (iXon3; Andor). In the wide-field fluorescence imaging mode, the bacteria were illuminated through 485/20 (centre wavelength/bandwidth in nanometres) excitation filter and the fluorescence emission was collected using 521/25 emission filter. All fluorescence images and videos of bacterial cells suspended in microdroplets were acquired with the integration time of 70 ms and the frame rate of video recording was 12.5 frames per second.

Determination of intracellular concentration of Venus fluorescent protein

Intracellular concentration of Venus fluorescent protein expressed in BL21 *E. coli* cells was determined by comparing the intensity of fluorescence emission from the cells and from a thin layer of Venus solution with a known concentration. To this end, both Venus solution and bacterial suspension samples were loaded into thin flow chambers formed by a glass cover slip and a microscope slide attached together by double-sided tape of 76 μm thickness. The flow chambers were first pre-treated at 100 °C for 10 min with 0.5 % poly-L-lysine solution in 50 mM phosphate buffer and, subsequently, 20 μL of Venus and Venus-expressing bacterial suspension were injected into the respective flow chambers. The bacteria were allowed to attach to the poly-L-lysine-coated surface for 20 minutes and the unattached cells

were then washed away using 50 mM phosphate buffer. Before recording fluorescence images from the samples, reference background image of a non-fluorescent (blank) sample was acquired with 200 ms exposure time; this image served to correct for the effects of CCD dark current and stray light (Fig. S3a, left). Subsequently, images of Venus solution were recorded using wide-field excitation with 473 nm laser light and the same exposure time as used for the background image acquisition (Fig. S3b, left). Finally, fluorescence images of adherent BL21 cells were recorded using the same excitation laser power and exposure time as for the Venus solution (Fig. S3c, left). After recording the images, histograms of pixel intensity values within an identical region selected in all images were generated (Fig. S3a-c, right). For this purpose, all pixel intensity values were normalized with respect to the maximal pixel intensity in the bacteria image. For the case of adherent fluorescent bacteria, individual cells within the region of interest were first identified using particle analysis macro of ImageJ and the pixel intensity was only evaluated within the image areas corresponding to the cells. Total of 100 bacteria were included in the histogram of Fig. S3c which features a relatively narrow peak centred at the normalized fluorescence intensity $\nu_B = 0.74$, indicating uniform level of protein expression in the cells. For the Venus solution with concentration $c_V = 1.5 \mu\text{M}$, pixel intensity histogram is centred at $\nu_V = 0.30$, below the emission level of the Venus-expressing BL21 cells (Fig. S3b). In order to estimate the intracellular concentration of Venus, difference in thickness of the bacteria and the fluorescent protein layer has to be taken into account. In our calculation, we assumed a typical bacteria thickness d_B of $0.6 \mu\text{m}$ and thickness of the Venus layer $d_V = 76 \mu\text{m}$ (thickness of the used double-sided tape). The approximate concentration c_B of Venus in the bacteria was then calculated as:

$$c_B = c_V \left(\frac{\nu_B}{\nu_V} \right) \left(\frac{d_V}{d_B} \right) \quad \text{S.1}$$

For the above given experimental values of c_V , ν_B , ν_V , d_V , and d_B , the concentration of Venus in the cells estimated from Eq. (S.1) is $c_B \approx 470 \mu\text{M}$.

Dependence of full width at half maximum of whispering gallery modes on the pump fluence and Venus photobleaching

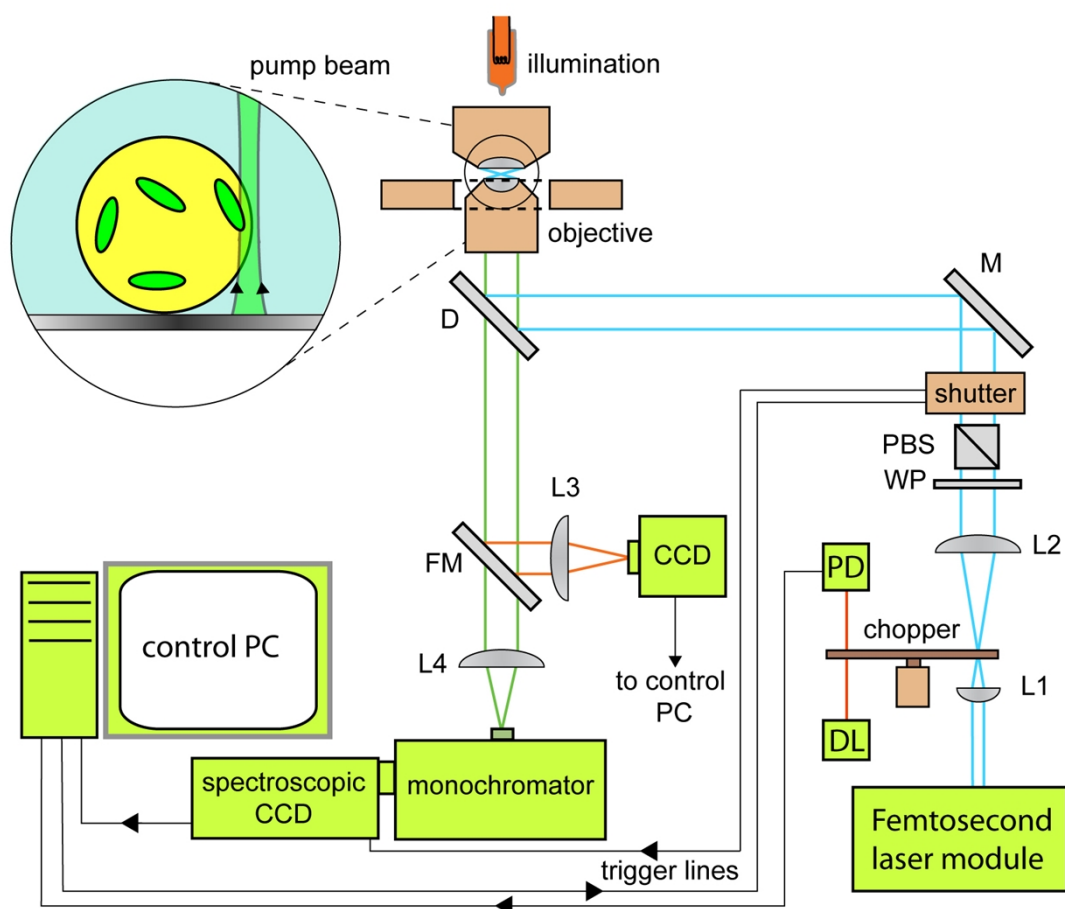
Due to nonlinear interactions between the amplified resonant light and Venus molecules inside the droplet cavity, full width at half maximum (FWHM) of lasing whispering gallery modes (WGMs) decreases upon crossing the threshold pump fluence required for lasing. Figure S4 shows FWHM of the lasing (part **a**) and reference (part **b**) WGMs studied in Fig. 2 of the manuscript as a function of the pump laser fluence. For illustration, intensity above background of the lasing WGM is also displayed. The analysis presented in the manuscript yielded the threshold pump fluence of 44.5 mJ/cm^2 for this particular droplet. From Fig. S4a, it follows that FWHM of the lasing WGM drops by approximately 20%, from 0.22 nm to 0.18 nm, when the pump threshold value is exceeded. This decrease of the mode FWHM correlates with a steeper increase of the WGM intensity with the pump fluence. In contrast, FWHM of the reference WGM which does not experience stimulated emission does not change systematically with increasing pump fluence; instead, it oscillates around the value of ~ 0.65 nm (Fig. S4b). A similar transition from the lasing to the non-lasing droplet emission regime was observed in Fig. 3 of the manuscript where the WGM intensity was analyzed as a function of the Venus photobleaching level. In Fig. S5, corresponding analysis of the WGM width is presented. For the lasing WGM (Fig. S5a), the intensity displays a quick initial decrease (characteristic decay time of $4.5 \mu\text{s}$) during which the mode nature gradually changes from lasing to spontaneous emission. This transition is clearly reflected in the sharp rise of the mode FWHM within the first three recorded spectral frames (cumulative exposure of $15 \mu\text{s}$), after which the mode FWHM stabilizes and increases only slightly. On the other

hand, the reference WGM does not show any sudden changes of FWHM and broadens only slowly with the cumulative exposure time (Fig. S5b).

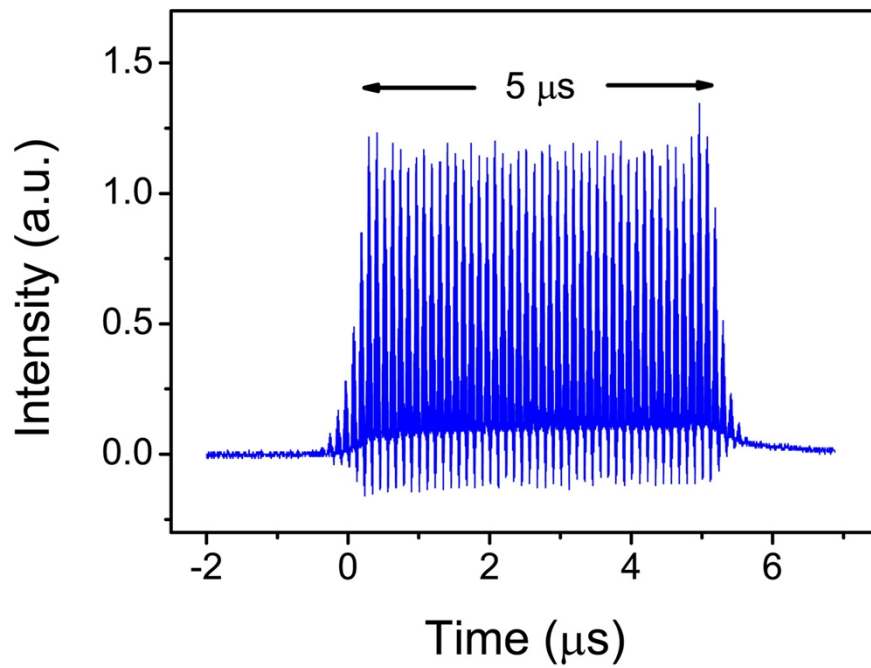
Fluorescence emission from surface-supported microdroplets containing Venus-expressing bacteria

Our optofluidic biolasers with live-cell gain medium are based on surface-supported glycerol-water microdroplets containing *E. coli* bacteria expressing Venus fluorescent protein. Figure S6 shows a differential interference contrast (DIC) image (Fig. S6a) and a fluorescence image (Fig. S6b) of a typical microdroplet used in the biolasing experiments. A group of bacterial cells located near the droplet centre is clearly visible in both images. In addition, the fluorescence image reveals presence of additional bacteria in the vicinity of the droplet surface; these bacterial cells can serve as the laser gain medium as they can efficiently couple to the droplet WGMs. In order to verify that the fluorescence is emitted solely from the bacteria, we recorded control images of glycerol-water microdroplets without the bacteria (see Figs. S6c and S6d). Comparison of fluorescence images of Figs. S6b and S6d acquired with the same illumination intensity and integration time of 70 ms clearly illustrates the absence of any appreciable fluorescence signal in the case of droplets that do not contain bacteria. Thus, we can rule out the contribution of the droplet liquid to the observed lasing spectra.

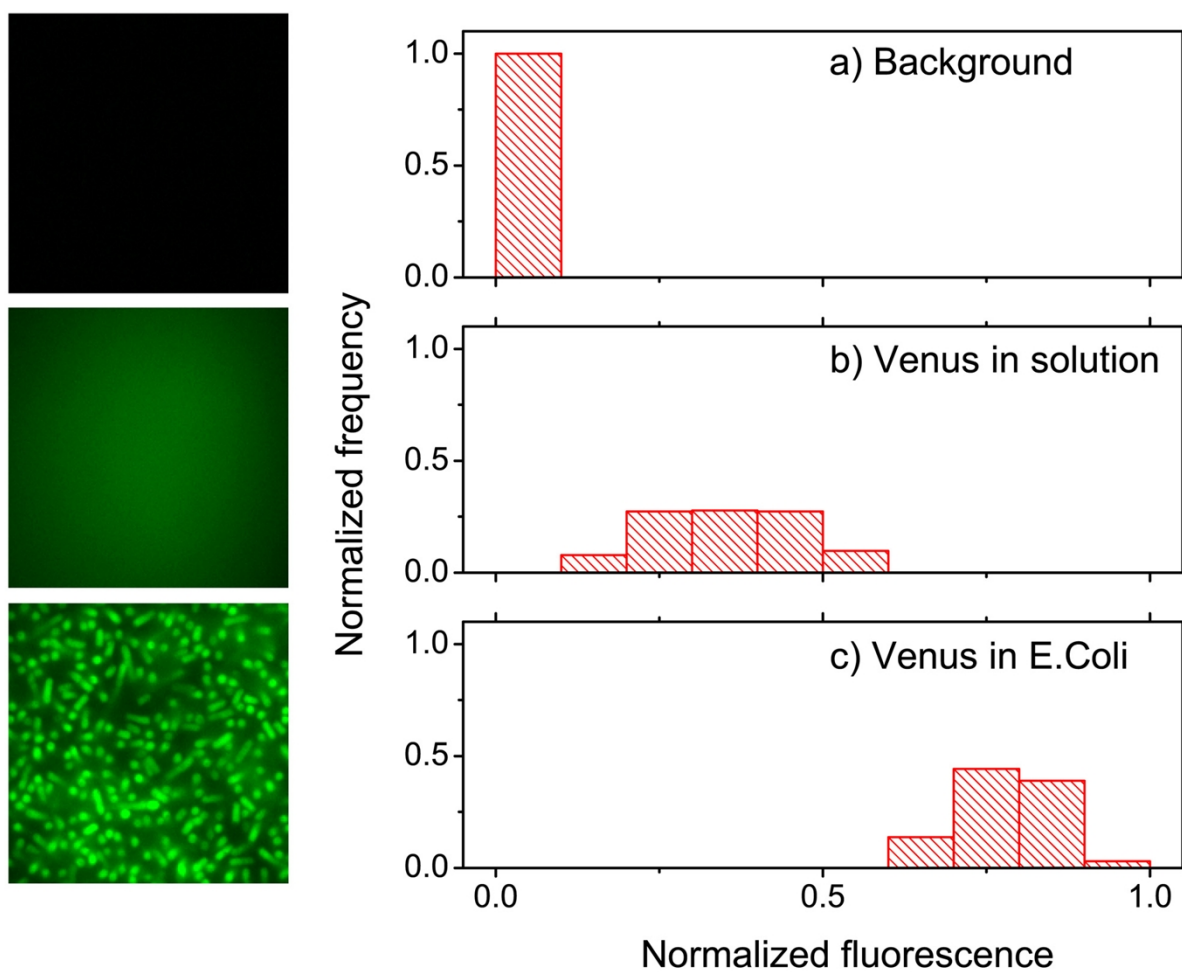
Supplementary figures



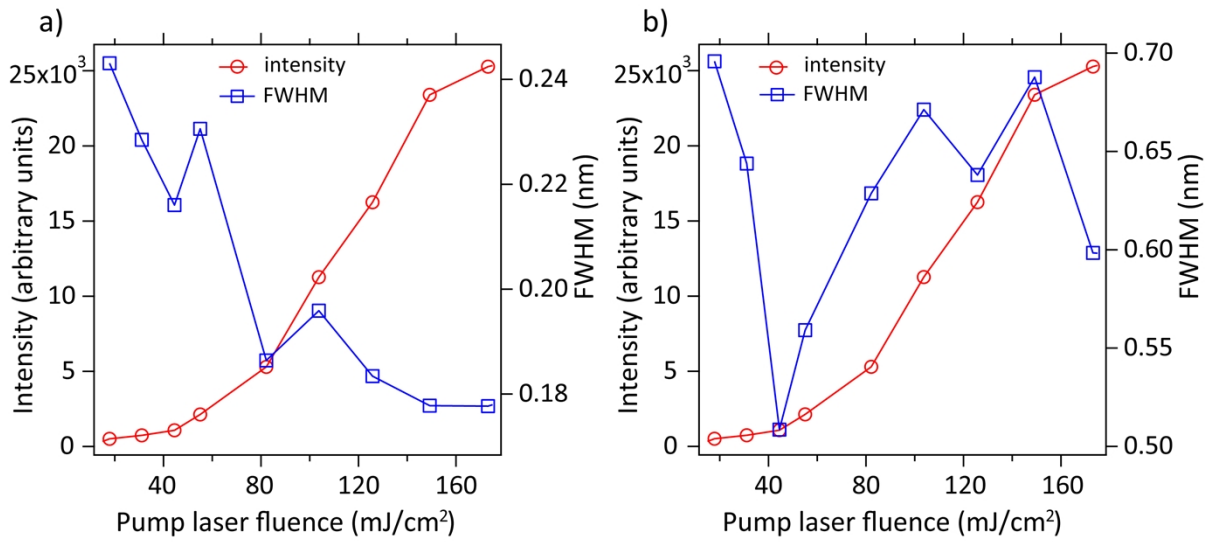
Supplementary Figure S1: Experimental setup for fluorescence spectroscopy of surface-supported lasing microdroplets. D – dichroic mirror, DL – diode laser module, FM – flippable mirror, L1 – L4 – lenses, M – mirror, PBS – polarizing beam splitter, PD – photodetector, and WP – $\lambda/2$ wave plate.



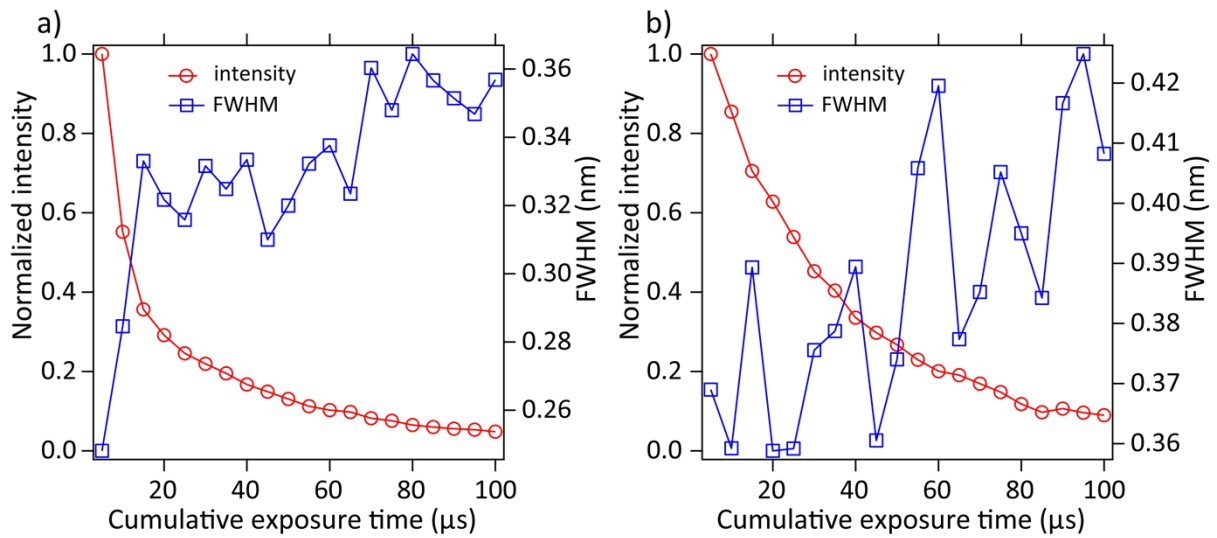
Supplementary Figure S2: A bunch of ~ 400 pulses from the pump laser beam with the pulse repetition rate of 80 MHz after transmission through a rotating chopper wheel with $\sim 155 \mu\text{m}$ diameter pinhole.



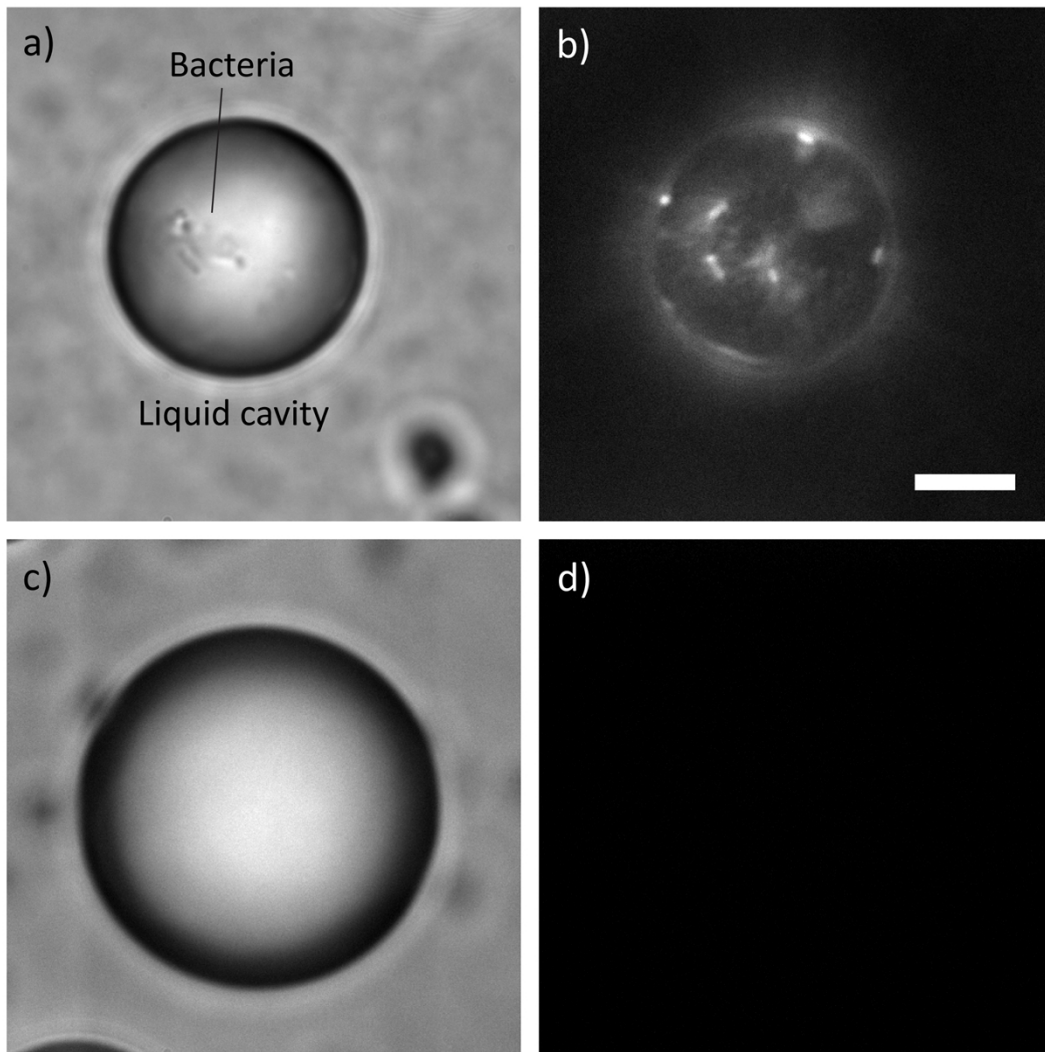
Supplementary Figure S3: **a**, Background image (left) and histogram of normalized pixel intensity values in this image (right). **b**, Fluorescence image of 1.5 μM Venus solution (left) and histogram of normalized pixel intensity values in this image (right). **c**, Fluorescence image of Venus-expressing BL21 *E. coli* cells adhering to cover slip surface (left) and histogram of normalized pixel intensity values over 100 cells selected in the image (right). Acquisition time for all images was 200 ms. Histograms are normalized such that the sum of frequencies of all bins is equal to 1.



Supplementary Figure S4: **a**, FWHM of the lasing WGM studied in Fig. 2 of the manuscript as a function of the pump laser fluence (squares). **b**, FWHM of the reference WGM studied in Fig. 2 of the manuscript as a function of the pump laser fluence (squares). In both figure parts, circles denote the intensity above background of the lasing WGM.



Supplementary Figure S5: **a**, FWHM of the lasing WGM studied in Fig. 3 of the manuscript as a function of the cumulative exposure time (squares). Circles denote the normalized intensity above background of this WGM. **b**, FWHM of the reference WGM studied in Fig. 3 of the manuscript as a function of the cumulative exposure time (squares). Circles denote the normalized intensity above background of this WGM.



Supplementary Figure S6: **a**, DIC image of a surface-supported glycerol-water microdroplet with suspended *E. coli* bacteria expressing Venus fluorescent protein. **b**, Fluorescence image of the same microdroplet as shown in **a**. **c**, DIC image of a surface-supported glycerol-water microdroplet without bacteria. **d**, Fluorescence image of the same microdroplet as shown in **c**. The scale bar is 10 μm .